DUPLICATE

METEOROLOGICAL OFFICE

Forecasting Research

Forecasting Research Division
Technical Report No. 122

Evaluation of a numerical scheme on a set of test problems for the shallow water equations

by

A.J. Malcolm

October 1994

Meteorological Office
London Road
Bracknell
Berkshire
RG12 2SZ
United Kingdom

ORGS UKMO F
National Meteorological Library
FitzRoy Road, Exeter, Devon. EX1 3PB

Forecasting Research Technical Note No. 122

Evaluation of a numerical scheme on a set of test problems for the shallow water equations.

A. J. Malcolm

October 1994

This document has not been published. Permission to quote from it must be obtained from the director of Forecasting Research.

© Crown Copyright 1994.

Evaluation of a numerical scheme on a set of test problems for the shallow water equations. [1]

A.J. Malcolm

Second Interim Report

Department of Mathematics

P.O.Box 220

University of Reading

Whiteknights

Reading

RG6 2AX

United Kingdom

[1]The work reported here forms part of the research programme of the Oxford/Reading Institute for Computational Fluid Dynamics and was supported by the Met. Office, Bracknell under contract MET 2a/0471.

Abstract

All predictive models used in numerical weather prediction involve the treatment of advective terms. In a previous report the advection scheme employed in the "unified model" which is used by the Met Office for numerical weather prediction was tested against other advection schemes in isolation on a standard test problem. In this report the full numerical method used in the "unified model" is evaluated on standard test problems for the Shallow Water Equations. As well as the operational procedure, possible alternative strategies are considered, the results compared and conclusions drawn as to what changes could be made to the operational procedure.

1 Introduction

All predictive models used in numerical weather prediction involve the numerical treatment of advective terms. In a previous report (Malcolm (1994)) the advection scheme (Cullen and Davies (1991)) in the "unified model" used by the Met Office was tested in isolation against other advection schemes on a standard test problem, posed in Williamson et al. (1992), hereafter known as W92, for the Shallow Water Equations (SWE). In this report the full numerical method (Cullen, Davies and Mawson (1993), hereafter known as DP10) used in the "unified model" is evaluated on the remainder of the standard test problems in W92. Each set of initial data in W92 either tests a particular part of the code or introduces a new feature into the problem. As well as the operational procedure in DP10, possible alternative strategies are considered, the results compared and conclusions drawn as to what changes might be made to the operational procedure.

2 The Equations

In this section we adapt the equations in the unified model documentation paper, DP10, to apply to the SWE on a sphere.

The major differences between these equations and those in DP10 are that here there is no vertical velocity and there is only one h level in the vertical, which means that the the k subscripts in DP10 can be ignored. The quantities θ (virtual potential temperature,) and Φ (topographic height) do not arise in the SWE. For clarity the i, j spatial subscripts are suppressed.

Consider then the SWE on the sphere, which are

$$\frac{\partial u}{\partial t} + \frac{u}{a\cos\phi}\frac{\partial u}{\partial \lambda} + \frac{v}{a}\frac{\partial u}{\partial \phi} - \left(f + \frac{u}{a}tan\phi\right)v + \frac{g}{a\cos\phi}\frac{\partial h}{\partial \lambda} = 0, \tag{1}$$

$$\frac{\partial v}{\partial t} + \frac{u}{a\cos\phi}\frac{\partial v}{\partial \lambda} + \frac{v}{a}\frac{\partial v}{\partial \phi} + \left(f + \frac{u}{a}tan\phi\right)u + \frac{g}{a}\frac{\partial h}{\partial \phi} = 0, \tag{2}$$

and

$$\frac{\partial h}{\partial t} + \nabla.(h\boldsymbol{u}) = 0, \tag{3}$$

where h is the height, (λ, ϕ) are the spherical coordinates, u, v are the velocities in the λ and ϕ coordinate directions respectively with $\boldsymbol{u} = (u, v)^T$, g is gravity and a is the radius of the earth.

The computational grid used is an Arakawa 'B' grid. The grid axes are in the λ and ϕ directions. The grid is N_λ by N_ϕ points, giving $\Delta\lambda = 2\pi/N_\lambda$ and $\Delta\phi = \pi/(N_\phi - 1)$ where

$\lambda \in [0, 2\pi]$ and $\phi \in [-\pi/2, \pi/2]$, with $\phi = 0$ the equator, $\phi = \pi/2$ the North Pole and $\phi = -\pi/2$ the South Pole. This means that the North Pole is actually represented by a line of N_λ points, i.e. the grid line j=1. The Arakawa B grid holds the values of the height field at each grid point with the velocity field being held at the centre of each grid cell. The height field is therefore an array of dimension N_λ by N_ϕ, whilst the velocity field is an array of dimension N_λ by $N_\phi - 1$. The grid size used for most of the results in this paper is 96x73. However some practical simulations are run on grids up to a size of 288x217 points.

In the discretisations the following notation is used for differences and averages:-

$$\delta_\lambda X = \frac{[X(\lambda + \frac{1}{2}\Delta\lambda) - X(\lambda - \frac{1}{2}\Delta\lambda)]}{\Delta\lambda},$$

$$\overline{X}^{\lambda} = \frac{1}{2}[X(\lambda + \frac{1}{2}\Delta\lambda) + X(\lambda - \frac{1}{2}\Delta\lambda)],$$

$$\overline{X}^{3\lambda} = \frac{1}{2}[X(\lambda + \frac{3}{2}\Delta\lambda) + X(\lambda - \frac{3}{2}\Delta\lambda)],$$

$$\overline{X}^{\lambda\phi} = \overline{\overline{X}^{\lambda}}^{\phi}.$$

Equations (1) and (2) are now split into an adjustment step and an advection step. The advection step solves $\frac{\partial \boldsymbol{u}}{\partial t} = -\boldsymbol{u}.\nabla\boldsymbol{u}$ while the adjustment step solves the remaining terms in equations (1) and (2).

The elements of equations (1) and (2) which form the adjustment step are manipulated to form a pair of coupled equations,

$$u^{n+1} = u^n + \delta t \left[\frac{1}{2}F_n(v^{n+1} + v^n) - \frac{g}{a\cos\phi}\overline{\delta_\lambda h^n}^{\phi}\right], \tag{4}$$

$$v^{n+1} = v^n - \delta t \left[\frac{1}{2}F_n(u^{n+1} + u^n) + \frac{g}{a}\overline{\delta_\phi h^n}^{\lambda}\right] \tag{5}$$

where

$$F_n = f + \frac{u^n}{a}tan\phi \qquad \text{and} \qquad f = 2\Omega\sin\phi_A. \tag{6}$$

Eliminating u^{n+1} from equations (4) and (5) gives

$$v^{n+1} = \frac{v^n\left[1 - \frac{\delta t^2}{4}F_n^2\right] - \frac{\delta t}{2}\left\{2F_n u^n + \frac{2g}{a}\overline{\delta_\phi h^n}^{\lambda} - \frac{g\delta t}{a\cos\phi}\overline{\delta_\lambda h^n}^{\phi}F_n\right\}}{\left(1 + \frac{\delta t^2}{4}F_n^2\right)}$$

while eliminating v^{n+1} from equations (4) and (5) gives a corresponding expression for u^{n+1}.

Before the remaining terms in equations (1) and (2) can be employed in the advection step it is necessary to calculate a new height field, h^{n+1}, which can be found using the time stepping,

$$h^{n+1} = h^n - \frac{\delta t}{a^2}D, \tag{7}$$

where

$$D = \frac{a}{\cos\phi}(\overline{\delta_\lambda(u\overline{h}^{\lambda\phi})}^{\phi} + \overline{\delta_\phi(v\overline{h}^{\lambda\phi}\cos\phi)}^{\lambda}), \tag{8}$$

gives a numerical approximation to $\nabla.(h\boldsymbol{u})$.

The treatment of the terms in equations (1) and (2) other than $-\boldsymbol{u}.\nabla\boldsymbol{u}$can now be implemented during the advection step. In the advection step a new vector $\boldsymbol{U}$ is defined which is an averaged height weighted velocity field, namely

$$\boldsymbol{U} = (U, V) = \frac{\sum_{i=1}^{N_A}(au_i\overline{h_i}^{\lambda\phi}, av_i\cos\phi\overline{h_i}^{\lambda\phi})}{N_A} \tag{9}$$

where N_A is the number of adjustment steps.

The fourth order Heun scheme as implemented by Cullen and Davies (1991) is then used to produce a new value for u and v giving the following equations,

$$\begin{aligned} a^2\overline{h^n}^{\lambda\phi}u^{\#} &= a^2\overline{h^n}^{\lambda\phi}u^n - \\ &\frac{\Delta t}{\cos\phi}\left((1+\nu)\overline{\overline{U}^{\lambda\phi^\phi}\delta_\lambda u}^{\lambda} + (1+\nu)\overline{\overline{V}^{\lambda\phi^\lambda}\delta_\phi u}^{\phi} - \nu\overline{\overline{U}^{\lambda\phi^\phi}\delta_\lambda u}^{3\lambda} - \nu\overline{\overline{V}^{\lambda\phi^\lambda}\delta_\phi u}^{3\phi}\right) \end{aligned} \tag{10}$$

$$\begin{aligned} a^2\overline{h^n}^{\lambda\phi}v^{\#} &= a^2\overline{h^n}^{\lambda\phi}v^n - \\ &\frac{\Delta t}{\cos\phi}\left((1+\nu)\overline{\overline{U}^{\lambda\phi^\phi}\delta_\lambda v}^{\lambda} + (1+\nu)\overline{\overline{V}^{\lambda\phi^\lambda}\delta_\phi v}^{\phi} - \nu\overline{\overline{U}^{\lambda\phi^\phi}\delta_\lambda v}^{3\lambda} - \nu\overline{\overline{V}^{\lambda\phi^\lambda}\delta_\phi v}^{3\phi}\right), \end{aligned} \tag{11}$$

$$a^2\overline{h^{n+1}}^{\lambda\phi}u^{n+1} = a^2\overline{h^{n+1}}^{\lambda\phi}u^n - \frac{\Delta t}{2}\left(\overline{\left(\frac{h^{n+1}}{h^n}\right)}^{\lambda\phi}\boldsymbol{U}.\nabla u^n + \boldsymbol{U}.\nabla u^{\#}\right) \tag{12}$$

$$a^2\overline{h^{n+1}}^{\lambda\phi}v^{n+1} = a^2\overline{h^{n+1}}^{\lambda\phi}v^n - \frac{\Delta t}{2}\left(\overline{\left(\frac{h^{n+1}}{h^n}\right)}^{\lambda\phi}\boldsymbol{U}.\nabla v^n + \boldsymbol{U}.\nabla v^{\#}\right), \tag{13}$$

where ν is defined as $\nu = \nu_b(1-\xi_{\max}^2)$. The choice $\nu_b = 0$ defines a 2nd order scheme and $\nu_b = \frac{1}{6}$ defines a 4th order scheme. The minimum value for ν is zero which gives 2nd order accurate space advection. The quantity $\xi_{\max}$ is defined as the maximum ξ along a line of latitude or longitude as appropriate, with ξ being defined by

$$\xi = (\frac{u^2\Delta t^2}{a^2\Delta\lambda^2\cos^2\phi} + \frac{v^2\Delta t^2}{a^2\Delta\phi^2})^{\frac{1}{2}}. \tag{14}$$

If required, diffusion of order $2j$ of any variable, X, may be added into the scheme using the additional term $(-1)^{j-1}D^jX$ where, for example, if $j = 3, D^3X = D(D(D(X)))$ and where $D(X)$ is defined by

$$D(X) = \frac{1}{a^2h^{n+1}}\left(\frac{1}{\cos^2\phi}\delta_\lambda(\overline{k_x(\lambda,\phi)}^{\phi}\delta_\lambda X) + \frac{1}{\cos\phi}\delta_\phi(\overline{k_y(\lambda,\phi)}^{\lambda}\cos\phi\delta_\phi X)\right) \tag{15}$$

with

$$k_y(\lambda,\phi) = h^{n+1}k \qquad\qquad k_x(\lambda,\phi) = k_y(\lambda,\phi)\left(\frac{\Delta\lambda\cos\phi}{\Delta\phi}\right)^2 \tag{16}$$

and k is a user chosen coefficient where for stability we require

$$\Delta t\left(\frac{4k}{a^2\Delta\phi^2}\right)^j \leq 1.$$

These are the main procedures implemented in a time-step of the numerical algorithm tested here, but there are other procedures mentioned in DP10. The grid splitting mentioned in Section 3.2 of DP10 is not implemented since the use of a 4th order advection scheme renders it redundant. Divergence damping is also not employed, but Fourier filtering is used to prevent the timestep being undesirably reduced by the short gridlengths used in high latitudes.

Fourier filtering is implemented to reduce the amplitude of unstable wavelengths in the numerical solution. The solution vector is reduced into its component waves each of which has a certain amplitude. If the timestep is such that the numerical solution is unstable at particular latitudes, then a criterion is used to determine which wavelengths are unstable and once the relevant wavelengths are found their amplitude is decreased by reducing the corresponding coefficients, or even setting the amplitude to zero (Fourier chopping). The solution vector is then reconstructed using the modified amplitudes.

The fourth order Heun scheme given in equations (10) to (13) is used in the advection step, although in the results presented here we not only produce results from the Heun scheme (as given in Malcolm (1994)) but also those from a simplified version of the Heun scheme and from a Lax-Wendroff scheme as well.

The simplified Heun scheme requires a new notation for differences as given below:

$$\delta_{2\lambda}X = \frac{[X(\lambda+\Delta\lambda) - X(\lambda-\Delta\lambda)]}{2\Delta\lambda}$$

together with $\boldsymbol{U} = (u,v)^T$.

The Heun scheme is then written as

$$u^{\#} = u^n - \frac{\Delta t}{a\cos\phi}\left(u^n\delta_{2\lambda}u^n + v^n\cos\phi\,\delta_{2\phi}u^n\right) \tag{17}$$

$$v^{\#} = v^n - \frac{\Delta t}{a\cos\phi}\left(u^n\delta_{2\lambda}v^n + v^n\cos\phi\,\delta_{2\phi}v^n\right), \tag{18}$$

$$u^{n+1} = u^n - \frac{\Delta t}{2a}\left(\boldsymbol{U}.\nabla u^n + \boldsymbol{U}.\nabla u^{\#}\right) \tag{19}$$

$$v^{n+1} = v^n - \frac{\Delta t}{2a}\left(\boldsymbol{U}.\nabla v^n + \boldsymbol{U}.\nabla v^{\#}\right). \tag{20}$$

In equations (19) and (20) the terms $\boldsymbol{U}.\nabla u^n$ and $\boldsymbol{U}.\nabla v^n$ are actually the terms inside the brackets in equations (17) and (18) respectively. The terms $\boldsymbol{U}.\nabla u^\#$ and $\boldsymbol{U}.\nabla v^\#$ are calculated exactly as in equations (17) and (18) but with u^n and v^n replaced by $u^\#$ and $v^\#$.

The Lax Wendroff scheme is slightly different in that the velocity values, $(u^\#, v^\#)$, are held on the h grid points. The scheme is:

$$u^\# = \overline{u^n}^{\lambda\phi} - \frac{\Delta t}{2a\cos\phi}\left(\overline{u^n}^{\lambda\phi}\overline{\delta_\lambda u}^{\phi} + \overline{v^n}^{\lambda\phi}\cos\phi\overline{\delta_\phi u}^{\lambda}\right) \tag{21}$$

$$v^\# = \overline{v^n}^{\lambda\phi} - \frac{\Delta t}{2a\cos\phi}\left(\overline{u^n}^{\lambda\phi}\overline{\delta_\lambda v}^{\phi} + \overline{v^n}^{\lambda\phi}\cos\phi\overline{\delta_\phi v}^{\lambda}\right), \tag{22}$$

$$u^{n+1} = u^n - \frac{\Delta t}{2a\cos\phi}\left(\overline{u^\#}^{\lambda\phi}\overline{\delta_\lambda u^\#}^{\phi} + \overline{v^\#}^{\lambda\phi}\cos\phi\overline{\delta_\phi u^\#}^{\lambda}\right) \tag{23}$$

$$v^{n+1} = v^n - \frac{\Delta t}{2a\cos\phi}\left(\overline{u^\#}^{\lambda\phi}\overline{\delta_\lambda v^\#}^{\phi} + \overline{v^\#}^{\lambda\phi}\cos\phi\overline{\delta_\phi v^\#}^{\lambda}\right). \tag{24}$$

3 The Test Cases

The problems investigated in this report are test cases 2 to 7 from W92. These are presented below together with an outline of what they set out to simulate. A reminder of test case 1 is also included so that a description of the complete suite is available. The suite of test cases includes an analytic problem to test the advection part of the scheme, steady state problems with analytic results, forced SWE, a problem with orography (surface topology) and finally a problem involving actual observed data.

3.1 Test Case 1

The first test case does not deal with the full SWE but solely with the advective part. It may be implemented in full shallow water codes by simply overwriting the calculated velocity field with the specified velocity field at all times.

This case is a test of the ability of the numerical scheme to cope with the transport of a disturbance around the globe. Different orientations of the advecting wind are specified. An initial height field is specified together with a velocity field which is analytically divergence free. The advecting wind is given by

$$u = u_0(\cos\phi\cos\alpha + \sin\phi\cos\lambda\sin\alpha), \tag{25}$$

$$v = -u_0\sin\lambda\sin\alpha, \tag{26}$$

where the parameter α is the angle between the axis of solid body rotation and the polar axis of the spherical coordinate system.

The initial height field is a cosine bell given by

$$h(\lambda,\phi) = \begin{cases} \frac{h_0}{2}(1+\cos(\frac{\pi r}{R})) & \text{if} \quad r < R \\ 0 & \text{if} \quad r \geq R, \end{cases} \tag{27}$$

where $h_0 = 1000\text{m}$, $R = a/3$, a is the radius of the earth and r is the great circle distance between (λ,ϕ) and the centre of the cone, which is initially at $(\lambda_c,\phi_c) = (3\pi/2, 0)$, where

$$r = a\cos^{-1}[\sin\phi_c \sin\phi + \cos\phi_c \cos\phi \cos(\lambda - \lambda_c)]. \tag{28}$$

The initial height field actually used is $h + h_0$, where h is as defined in (27). This point is important as in a number of places height weighted velocity fields are used in calculations and so if the height field is zero then the equations become undefined, see Malcolm (1994). For results of the tests see the previous report, Malcolm (1994).

3.2 Test Case 2

The second test case is a steady state solution of the SWE. It consists of zonal flow with the corresponding geostrophic height field. The advecting wind is at an angle α to the equator.

The velocity fields are initially, and for all time,

$$u = u_0(\cos\phi\cos\alpha + \cos\lambda\sin\phi\sin\alpha), \tag{29}$$

$$v = -u_0 \sin\lambda \sin\alpha, \tag{30}$$

while the analytic h field is given by

$$h = h_0 - \frac{u_0}{g}(a\Omega + \frac{u_0}{2})(\sin\phi\cos\alpha - \cos\lambda\cos\phi\sin\alpha)^2. \tag{31}$$

W92 suggest that it might be necessary to modify the initial wind and height field so that they satisfy a discrete geostrophic balance relationship. This discrete balance was implemented as was the analytic data. To satisfy discrete geostrophic balance we need

$$u = \frac{-g}{af}\overline{\delta_\lambda h}^{\phi}, \tag{32}$$

$$v = \frac{g}{af\cos\phi}\overline{\delta_\phi h}^{\lambda}. \tag{33}$$

The coriolis term f is given by

$$f = 2\Omega(\sin\phi\cos\alpha - \cos\lambda\cos\phi\sin\alpha). \tag{34}$$

The parameters used in the tests described here are $u_0 = 2\pi a/(12\text{days})$ and $h_0 = 2.94 \times 10^4/g$ while α takes the values, $\alpha = 0.0, 0.005, \frac{\pi}{2} - 0.005, \frac{\pi}{2}$.

The graphical results are presented below in Section 7 and discussed in Section 4.

3.3 Test Case 3

This case is similar to the previous one except that the wind field is only non-zero in a limited region. The easiest way to define the wind and height fields is to start with a (λ', ϕ') coordinate system coincident with the earth's rotation axis and then rotate it by an angle α to the coordinate system(λ, ϕ). Since it is difficult to write the equations straight down in the (λ, ϕ) system the fields are defined in stages.

The velocity components (u', v') are given by

$$u' = u_0 b(x) b(x_e - x) e^{4/x_e}, \tag{35}$$

$$v' = 0, \tag{36}$$

where

$$b(x) = \begin{cases} 0 & \text{if } x \leq 0 \\ e^{-x^{-1}} & \text{if } 0 < x \end{cases} \tag{37}$$

and

$$x = x_e(\phi' - \phi_b)(\phi_e - \phi_b)^{-1}. \tag{38}$$

The parameters are $u_0 = 2\pi a/(12\text{days}), \phi_b = \frac{-\pi}{6}, \phi_e = \frac{\pi}{2}$, and $x_e = 0.3$.

The velocity components u and v are defined as

$$v\cos\phi = -u'\sin\alpha\sin\lambda', \tag{39}$$

$$u\cos\lambda = v\sin\phi\sin\lambda + u'\cos\lambda', \tag{40}$$

with the coordinates related by

$$\sin\phi' = \sin\phi\cos\alpha - \cos\phi\cos\lambda\sin\alpha, \tag{41}$$

$$\sin\lambda'\cos\phi' = \sin\lambda\cos\phi. \tag{42}$$

Thus, if we know λ and ϕ, equation (41) lets us determine ϕ' since $\phi' \in [-\pi/2, \pi/2]$. Using this in equation (42) we can find $\sin\lambda'$, but since $\lambda' \in [0, 2\pi]$ we need to determine which quadrant λ' falls in and this can be calculated by ensuring that

$$\cos\phi = \sin\phi' \cos\alpha + \cos\phi' \sin\alpha \cos\lambda'. \tag{43}$$

The coriolis parameter is defined as

$$f = 2\Omega(\sin\phi\cos\alpha - \cos\lambda\cos\phi\sin\alpha). \tag{44}$$

and for a steady state solution h' must satisfy

$$\frac{(u')^2 \tan\phi'}{a} + \frac{g}{a}\frac{\partial h'}{\partial \phi'} + fu' = 0. \tag{45}$$

The height h is difficult to find analytically, so the form in the prime system

$$h = h_0 - \frac{a}{g}\int_{-\pi/2}^{\phi'} (2\Omega \sin\tau + \frac{u'(\tau)\tan\tau}{a}) u'(\tau)\delta\tau \tag{46}$$

is integrated numerically to give h. The quantity h_0 is the same as in test case 2.

The test case has been run with $\alpha = 0.0$ and $\pi/3$. The graphical results are presented below in Section 7 and discussed in Section 4.

3.4 Test Case 4

The non-linear steady state test cases, 2 and 3, are the simplest method of measuring the adequacy of a particular numerical method. The measure of performance of a scheme on the non-linear unsteady equations is also desirable, but analytic solutions are all but nonexistent. Thus a flow $\tilde{u}, \tilde{v}$ and $\tilde{h}$ that is similar in structure to those in the atmosphere is chosen. This flow is a solution of the forced shallow water system given below in equations (47) to (50).

The flow is a translating low pressure centre superimposed on a jet stream which is symmetrical about the equator. This field exhibits some of the properties of middle level tropospheric flow.

Test case 4 is a forced SWE problem which actually simulates the effect of a physics step in the unified model. If the forcing terms are thought of as corresponding to the correction due to the physics then, since the SWE are split into an "adjustment" step and an "advection" step, it is is possible to test whether the forcing terms should be added solely to the advection step or equally to each adjustment step.

The forced SWE are

$$\frac{du}{dt} - \left(f + \frac{u}{a}tan\phi\right)v + \frac{g}{a\cos\phi}\frac{\partial h}{\partial\lambda} = F_u, \tag{47}$$

$$\frac{dv}{dt} + \left(f + \frac{u}{a}tan\phi\right)u + \frac{g}{a}\frac{\partial h}{\partial\phi} = F_v, \tag{48}$$

$$\frac{dh}{dt} + \frac{h}{a\cos\phi}\left(\frac{\partial u}{\partial\lambda} + \frac{\partial v\cos\phi}{\partial\phi}\right) = F_h, \tag{49}$$

where the height of the mountains, h_s, is defined as zero and the substantive derivative is

$$\frac{d}{dt} = \frac{\partial}{\partial t} + \frac{u}{a\cos\phi}\frac{\partial}{\partial\lambda} + \frac{v}{a}\frac{\partial}{\partial\phi}. \tag{50}$$

The forcing terms in equations 47) to (49) are defined as

$$F_u = \frac{d\tilde{u}}{dt} - \left(f + \frac{\tilde{u}}{a}tan\phi\right)\tilde{v} + \frac{g}{a\cos\phi}\frac{\partial\tilde{h}}{\partial\lambda}, \tag{51}$$

$$F_v = \frac{d\tilde{v}}{dt} + \left(f + \frac{\tilde{u}}{a}tan\phi\right)\tilde{u} + \frac{g}{a}\frac{\partial\tilde{h}}{\partial\phi}, \tag{52}$$

$$F_h = \frac{d\tilde{h}}{dt} + \frac{\tilde{h}}{a\cos\phi}\left(\frac{\partial\tilde{u}}{\partial\lambda} + \frac{\partial\tilde{v}\cos\phi}{\partial\phi}\right). \tag{53}$$

The flow fields are given by

$$\tilde{u} = \bar{u} - \frac{\bar{\psi}_\phi}{a}, \tag{54}$$

$$\tilde{v} = \frac{\bar{\psi}_\lambda}{a\cos\phi}, \tag{55}$$

$$g\tilde{h} = g\bar{h} + f\bar{\psi}, \tag{56}$$

where

$$\bar{u} = u_0\sin^{14}(2\phi), \tag{57}$$

$$g\bar{h} = gh_0 - \int_{-\pi/2}^{\phi}[af(\tau) + \bar{u}(\tau)\tan\tau]\bar{u}(\tau)\partial\tau \tag{58}$$

and

$$\bar{\psi}(\lambda,\phi,t) = \psi_0 e^{-\sigma((1-C)/(1+C))} \tag{59}$$

with $\psi_0 = -0.03(gh_0/f_0), \sigma = (12.74244)^2, gh_0 = 10^5, f_0 = 2\Omega\sin(\pi/4)$, and

$$C = \sin\phi_0\sin\phi + \cos\phi_0\cos\phi\cos\left(\lambda - \frac{u_0}{a}t - \lambda_0\right). \tag{60}$$

The centre of the low is initially located at $(\lambda_0, \phi_0) = (0, \pi/4)$.

Results for this problem are not available due to coding difficulties in evaluating numerically all the terms in equations (51) to (60).

3.5 Test Case 5

This test case consists of zonal flow, as in test case 2, impinging on a mountain. The wind and height field are as in case 2 with $\alpha = 0$ but with $h_0 = 5960$ and $u_0 = 20$. The mountain height is given by

$$h_s = h_{s0}(1 - r/R), \tag{61}$$

where $h_{s0} = 2000, R = r/9$ and $r^2 = \min[R^2, (\lambda - \lambda_c)^2 + (\phi - \phi_c)^2]$. The centre is taken as $\lambda_c = 3\pi/2$ and $\phi_c = \pi/6$.

This tests the code when there is surface topology involved in the problem. In this case the surface is a steeply sloping mountain.

The graphical results are presented below in Section 7 and discussed in Section 4.

3.6 Test Case 6

Rossby-Haurwitz waves are analytic solutions of the nonlinear barotropic vorticity equation on the sphere. Although they are not analytic solutions of the SWE they have been used so long they are now *de-facto* standard test cases.

Test case 6 is the Rossby-Haurwitz wave with R=4. This problem is actually well suited to a spectral model and so any comparison between results from the finite difference scheme and from a spectral model would be unfairly weighted towards the spectral model.

This test case has a height field that moves from east to west with no change in shape, with an angular velocity v given by

$$v = \frac{R(R+3)\omega - 2\Omega}{(1+R)(2+R)}. \tag{62}$$

The velocity components are given by

$$u = a\omega\cos\phi + aK\cos^{R-1}\phi(R\sin^2\phi - \cos^2\phi)\cos R\lambda, \tag{63}$$

$$v = -aKR\cos^{R-1}\phi\sin\phi\sin R\lambda. \tag{64}$$

and the height is obtained from the stream function by solving the balance equation, so the initial tendency of the divergence is zero:

$$gh = gh_0 + a^2A(\phi) + a^2B(\phi)\cos R\lambda + a^2C(\phi)\cos 2R\lambda, \tag{65}$$

$$A(\phi) = \frac{\omega}{2}(2\Omega + \omega)\cos^2\phi + \frac{1}{4}K^2\cos^{2R}\phi[(R+1)\cos^2\phi + (2R^2 - R - 2) - 2R^2\cos^{-2}\phi], \tag{66}$$

$$B(\phi) = \frac{2(\Omega+\omega)K}{(R+1)(R+2)}\cos^R\phi[(R^2+2R+2)-(R+1)^2\cos^2\phi], \tag{67}$$

$$C(\phi) = \frac{1}{4}K^2\cos^{2R}\phi[(R+1)\cos^2\phi-(R+2)]. \tag{68}$$

The parameters are $\omega = K = 7.848 \times 10^{-6}$ and $h_0 = 8 \times 10^3$.

The graphical results are presented below in Section 7 and discussed in Section 4.

3.7 Test Case 7

This test case is comprised of 3 sets of initial data taken from physically observed data. The observations were made at the following times:-

- 0000 GMT December 21, 1978
- 0000 GMT January 16, 1979
- 0000 GMT January 9, 1979.

2D contour plots for the initial height fields are given later, see Figures 16, 19 and 22 respectively. These data sets test the code on a very unsymmetric problem.

The first data set has strong flow over the North pole and has pointed out deficiencies in schemes which have been applied to it by previous researchers. The second data set is characterised by two cutoff lows. The flow pattern develops into a typical blocking situation. The third data set initially has strong zonal flow.

The graphical results are presented below in Section 7 and discussed in Section 4.

4 Results and Comparisons

Results produced by the NCAR STSWM model (Hack and Jakob (1992)) are used in problems 5-7 as "reference solutions". These were retrieved by using the netcdf files provided by NCAR of their test runs. For a full comparison the paper by Heikes (1993) shows a full set of results as does the paper Jakob et al (1993).

A large number of test runs were carried out and a comparison of a number of different solution strategies were made.

The problem on which most of the results comparison was carried out was test case 6, the Rossby-Haurwitz problem with R=4. this is to allow comparison with others works as

the Rossby-Haurwitz problem has become almost a standard test case for any code. The results showed that a reasonable strategy could be formulated in conjunction with the numerical scheme presented in Cullen and Davies (1991). The alternative advection schemes tested, namely, simplified Heun and Lax-Wendroff, did not produce any satisfactory results as they became linearly unstable at high latitudes.

Figure 1 shows the initial data for the steady state test case 2 with the advecting wind angle being along the equator ($\alpha = 0$). Figure 2 shows the height field after 5 days and it can clearly be seen that the solution has remained almost unchanged. This reinforces the findings in the previous report (Malcolm (1994)) that flow in the equatorial direction is treated well by the numerical scheme. Figure 3 shows the initial data for another steady state test case 2 with the advecting wind angle being over the North Pole. Figure 4 shows that there has been some distortion of the height field and a small numerical oscillation has occurred in the polar region.

Figure 5 is the initial data for the non-linear steady-state test case 3 with $\alpha = \pi/3$. Figure 6 shows the results after 5 days with the filtering applied only to the velocity and height field. Figure 7 shows the corresponding result when the weighted velocity fields have been filtered. There is a slight difference between Figures 6 and 7 with the instabilities generated in Figure 7 being slightly larger than those in Figure 6.

The initial data for test case 5 is the same as in Figure 1 but there is underlying orography (a mountain). As stated above the NCAR STSWM code was used to produce reference solutions from a T213 grid. Figure 8 shows this reference solution while Figure 9 shows the solution generated by my code. The main features show a good correspondence in both figures. The only real difference is to the pole side of the mountain where the contours diverge slightly, see Figure 10.

The next set of figures is for the Rossby-Haurwitz R=4 case. Figure 11 shows the initial height field and Figure 12 shows the reference solution after 14 days, which has the same form but is just displaced along the equator. The results shown are a sample of the complete set. Figure 13 shows the result of running the test case with a 10 minute time step (this is the usual timestep). It is easy to see that the code has trouble coping with this as the peaks in the height field are starting to separate and go in different directions. Figure 14 shows what happens if we decrease the time step to 1 minute, the peaks do not split up and the main form of the solution is kept. The filtering in both these cases is of the fields themselves and there are no numerical instabilities being generated. Figure 15 shows the results on a 288×217 grid with a 2 minute

time step. There is a slight separation in the peaks which is developing and in this case a slight numerical instability is starting to occur near the poles.

The results for test case 7 are split into 3 sets. For each set of initial data the initial data is the first picture, the reference solution is the second picture and the third picture is the solution given by our code. The date of each initial data set is given on the picture of the initial data.

The first set is Figures 16 to 18. This exhibits a strong cross polar flow in the northern hemisphere. It is possible to see visually that the code has had trouble coping with this strong cross polar flow and that numerical instabilities have been introduced.

The second set is Figures 19 to 21. This represents a low in the northern hemisphere. It is possible to see that the low has been well tracked and that the southern hemisphere is well modelled, but again it is possible to see the introduction of numerical instabilities.

The third set is Figures 22 to 24. This is probably the best set of results as the main features in the reference solution also occur in the solution given by the unified model scheme and no numerical instability has been produced.

In the cases where numerical instabilities occur it is almost certainly due to the filtering being unable to stabilise the finite difference scheme in some latitudes.

5 Conclusions

In a number of cases the numerical scheme seems to be unable to cope in high latitude regions and introduces numerical instabilities into these regions. These numerical instabilities are then propagated through the whole solution region, since the numerical diffusion and filtering are unable to cope with such large instabilities.

The choice of diffusion coefficient is a factor in the accuracy of the results as the wrong diffusion coefficient can make a large difference.

The steady state test cases seem to be well modelled by the scheme and the introduction of orography in test case 5 is dealt with well. The Rossby-Haurwitz problem is modelled fairly well but changes in diffusion coefficient, filtering strategies and time step can change the results greatly. The final test case data sets show up the problem which the code has when dealing with very strong flow over the polar regions.

The overall conclusion is that the Heun scheme currently in use in the unified model is the best of the finite difference schemes available but it can be seen from the comparisons with

Semi-Lagrangian results in Malcolm (1994) that the Semi-Lagrangian scheme is likely to be an improvement.

The continuation of this work will focus on the new semi-implicit Semi-Lagrangian scheme which is to be introduced into the unified model and which will need to be validated.

6 Acknowledgements

I would like to thank the Meteorological Office for the funding of the contract under which I am working and Dr Mike Cullen, Dr Terry Davies and Mark Mawson there for their advice and helpful suggestions. I would also like to thank Dr Mike Baines and Dr Peter Sweby for useful discussions during the course of this work.

References

[1] **M.J.P. Cullen and T. Davies**, (1991), *A conservative split-explicit integration scheme with fourth-order horizontal advection*, J. R. Meteorol. Soc.**117**, pp 993-1002

[2] **M.J.P. Cullen, T. Davies and M.H. Mawson**, (1993), *Conservative Finite Difference Schemes for a Unified Forecast/Climate Model*, Met. Office Unified Model Documentation Paper No. 10, Version No. 24

[3] **J.J. Hack and R. Jakob**, (1992), *Description of a Global Shallow water Model Based on the Spectral Transform Method.*, NCAR Technical Note, NCAR/TN-343+STR

[4] **Ross P. Heikes and David A. Randall**, (1993) *The Shallow Water Equations on a Spherical Geodesic Grid*, Colorado State University, Dept. Atm. Sci Paper, 524

[5] **R. Jakob, J.J. Hack and D.L. Williamson**, (1993), *Solutions to the Shallow Water Test Set Using the Spectral Transform Method*, NCAR Technical Note, NCAR/TN-388-STR

[6] **A.J. Malcolm**, (1994), *Testing advection schemes for the shallow water equations on a set of test problems, I*, Met. Office Forecasting Research Technical Note No. 83

[7] **D.L. Williamson, J.B. Drake, J.J. Hack, R. Jakob and P.N. Swarztrauber**, (1992), *A Standard Test Set for Numerical Approximations to the Shallow Water Equations in Spherical Geometry*, J. Comp. Phys. **102**, pp 211-224

7 Figures

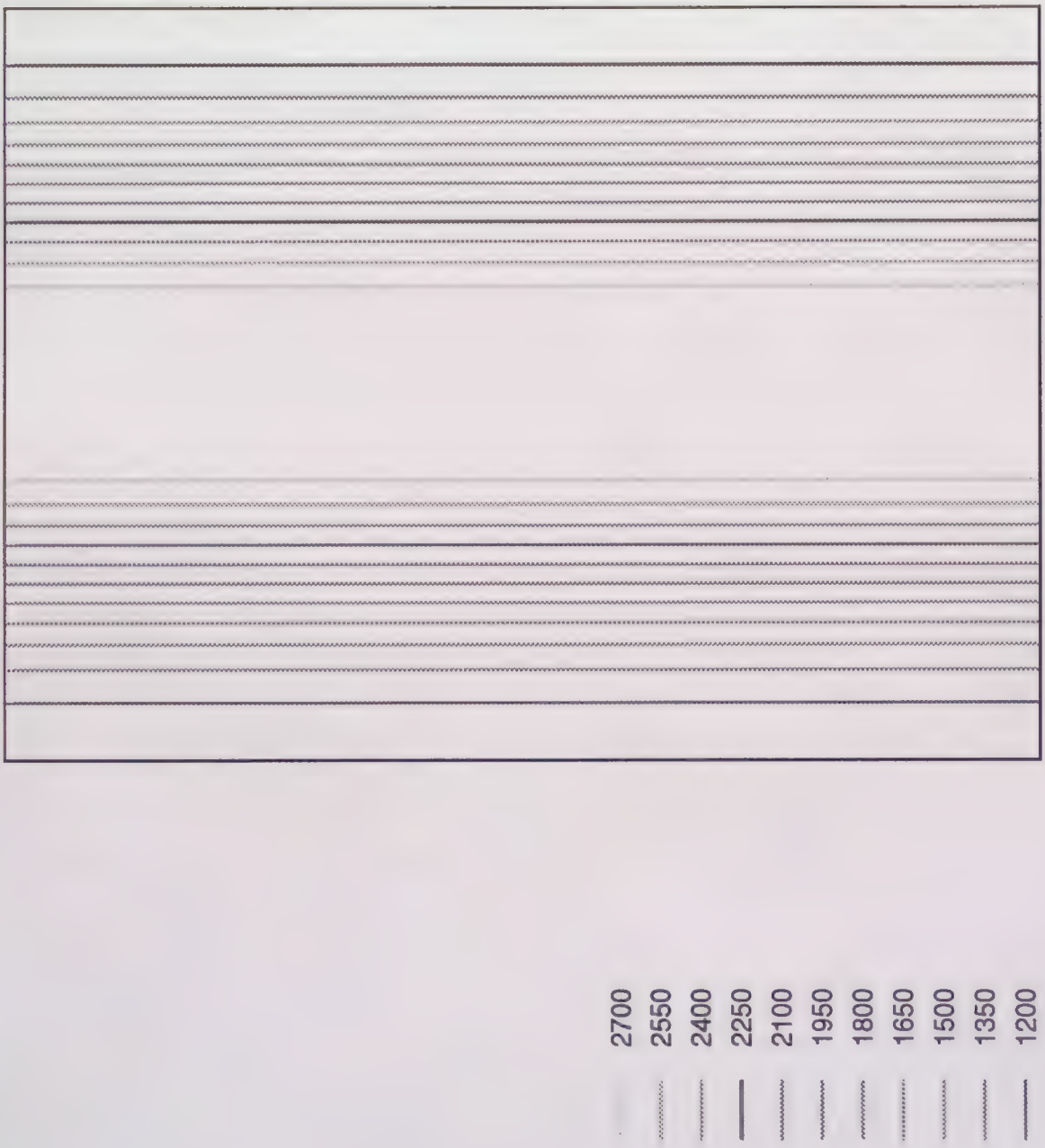

Figure 1: Test case 2, initial height field, $\alpha = 0$

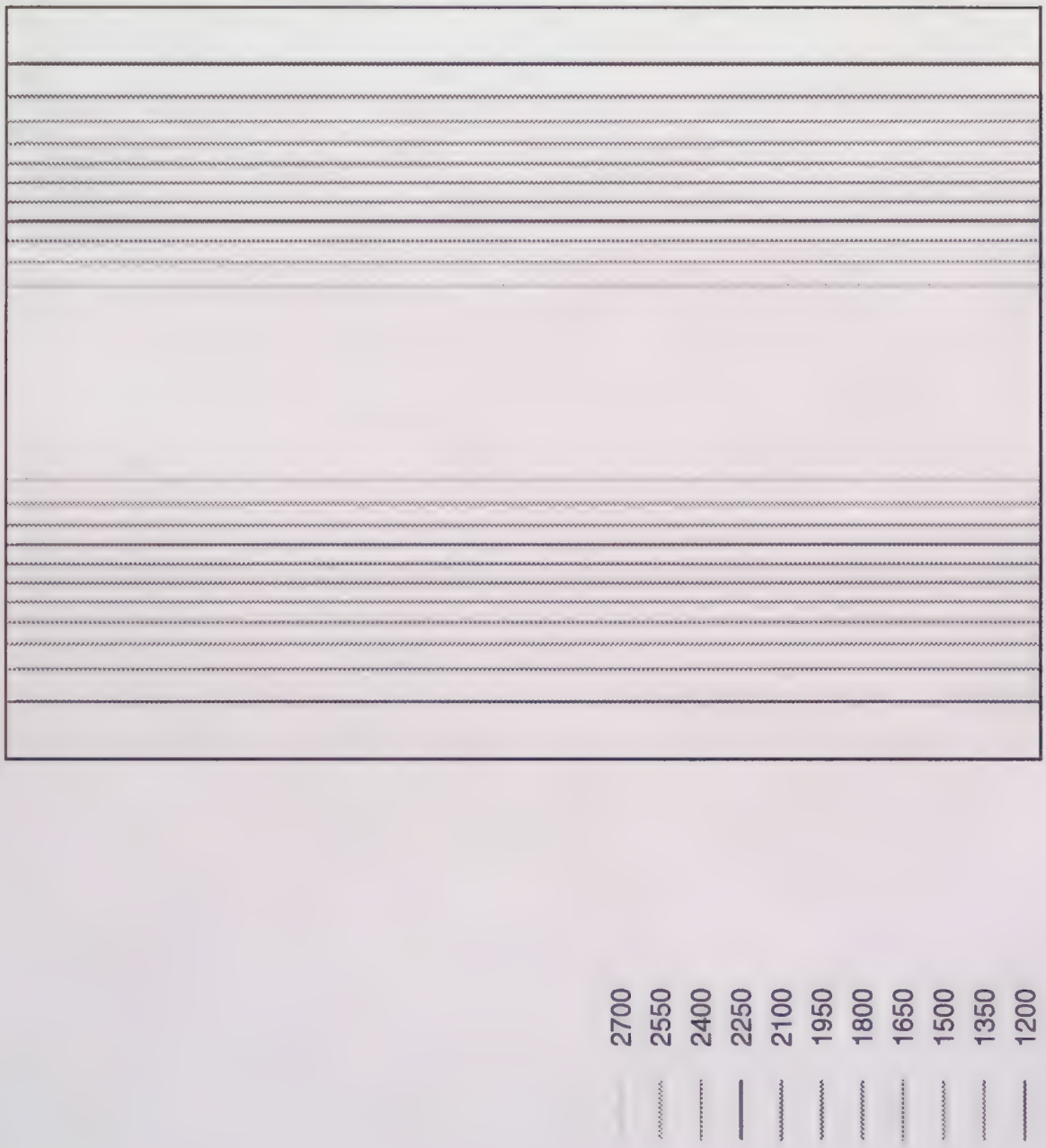

Figure 2: Test case 2, height field after 5 days, $\alpha = 0$

Figure 3: Test case 2, initial height field, $\alpha = \pi/2$

Figure 4: Test case 2, height field after 5 days, $\alpha = \pi/2$

Figure 5: Initial height field for test case 3, $\alpha = \pi/3$

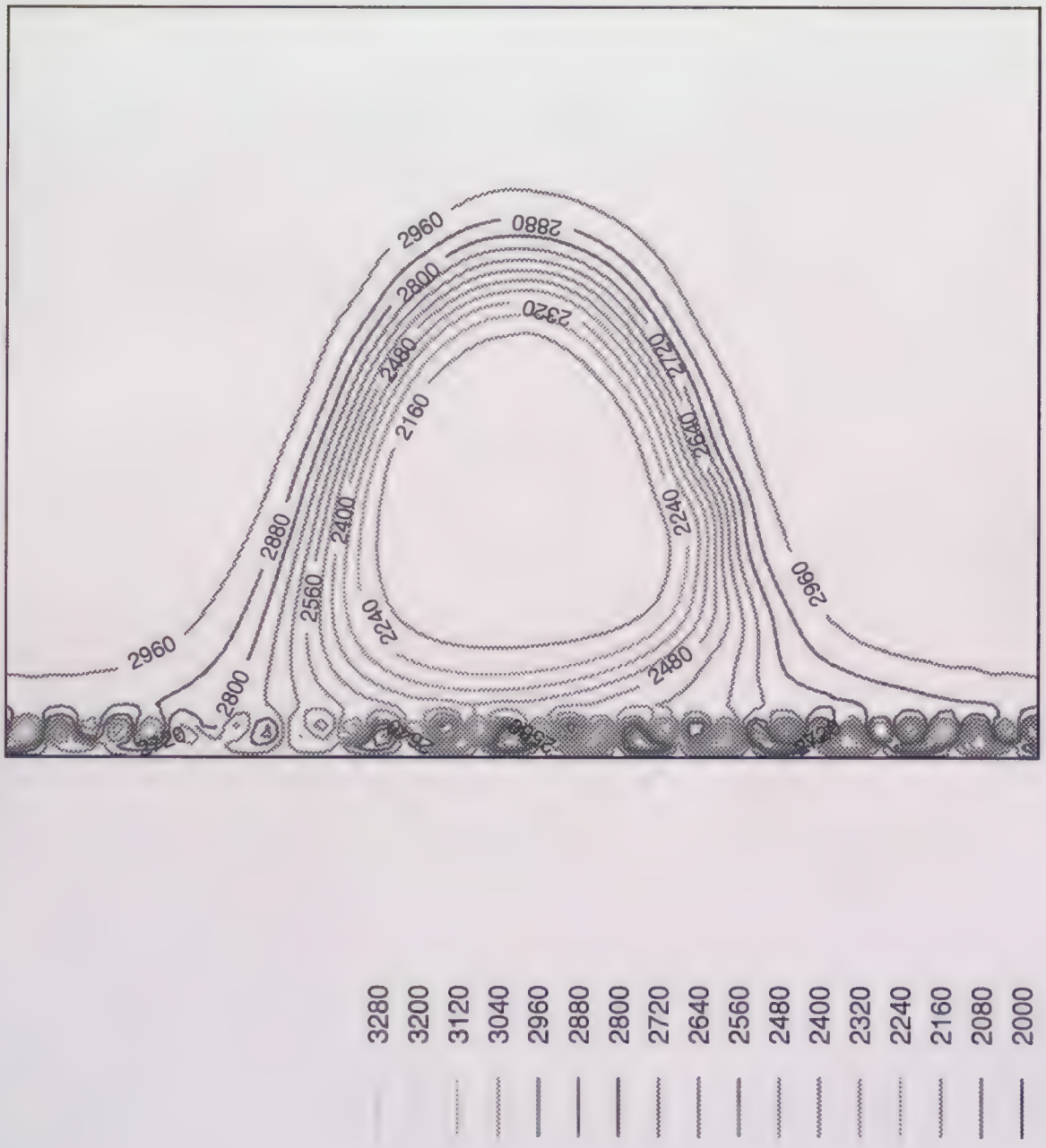

Figure 6: Test case 3, height field after 5 days, filtering fields only

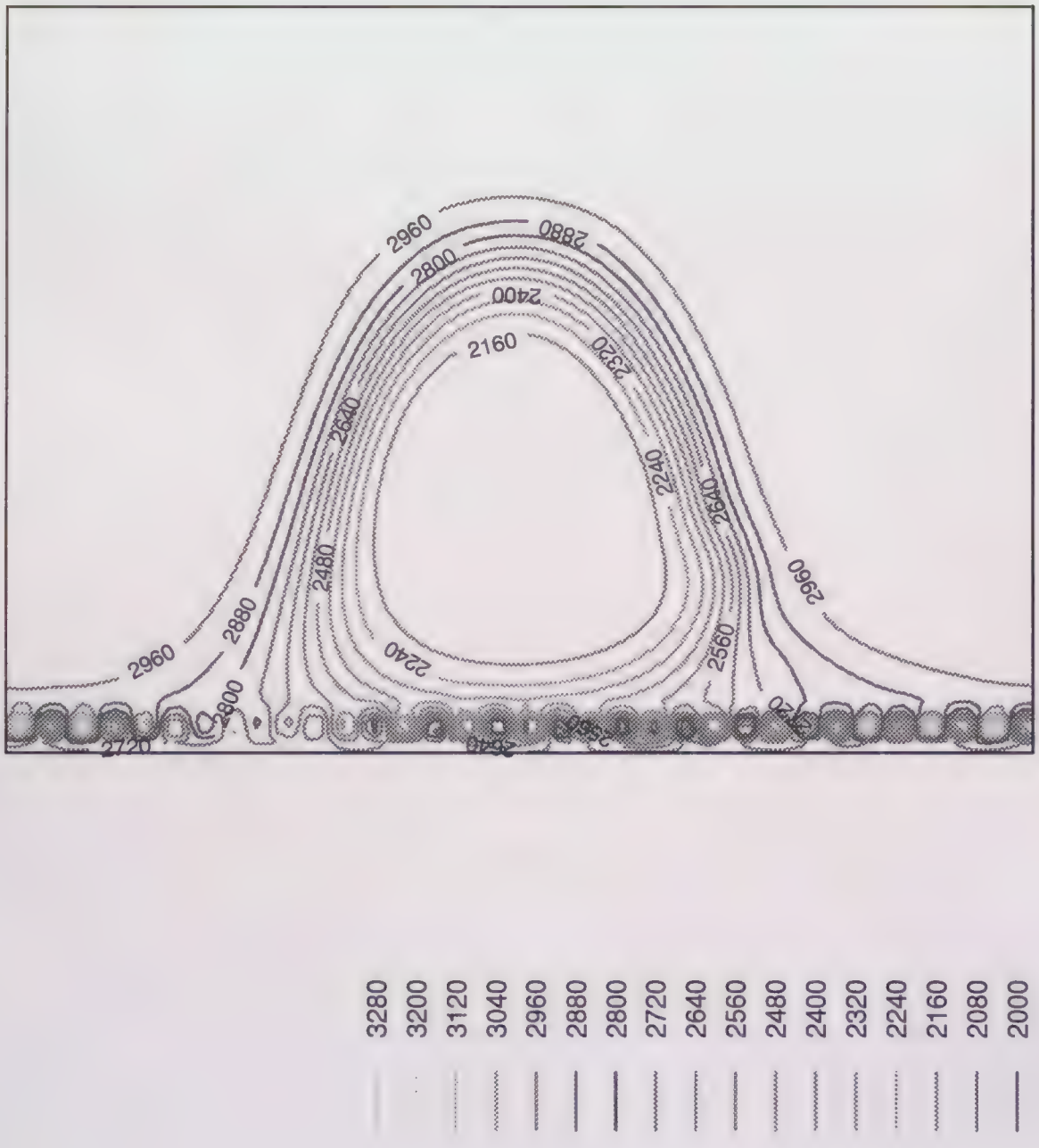

Figure 7: Test case 3, height field after 5 days, filtering weighted fields

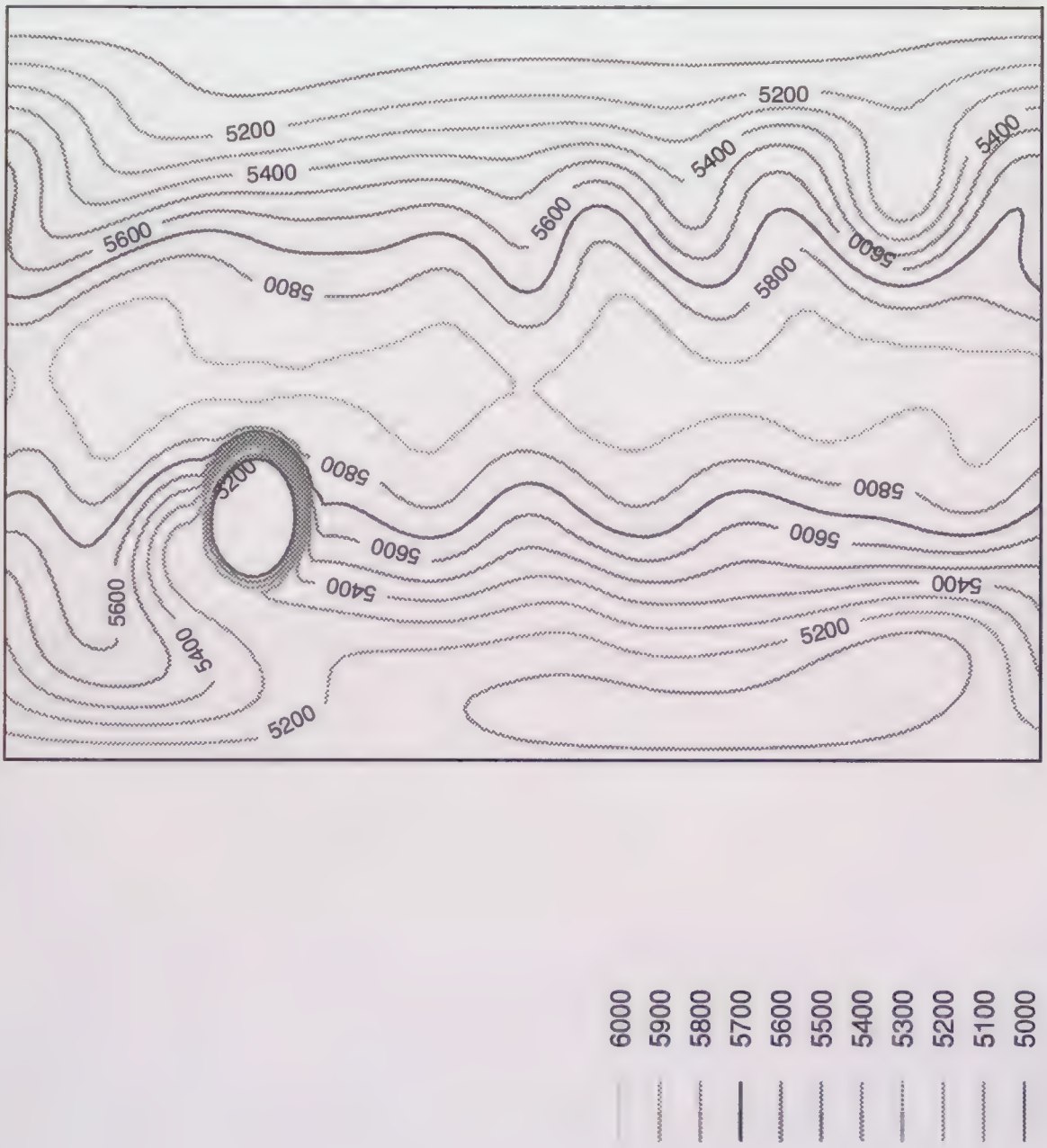

Figure 8: Test case 5, reference solution height field after 15 days

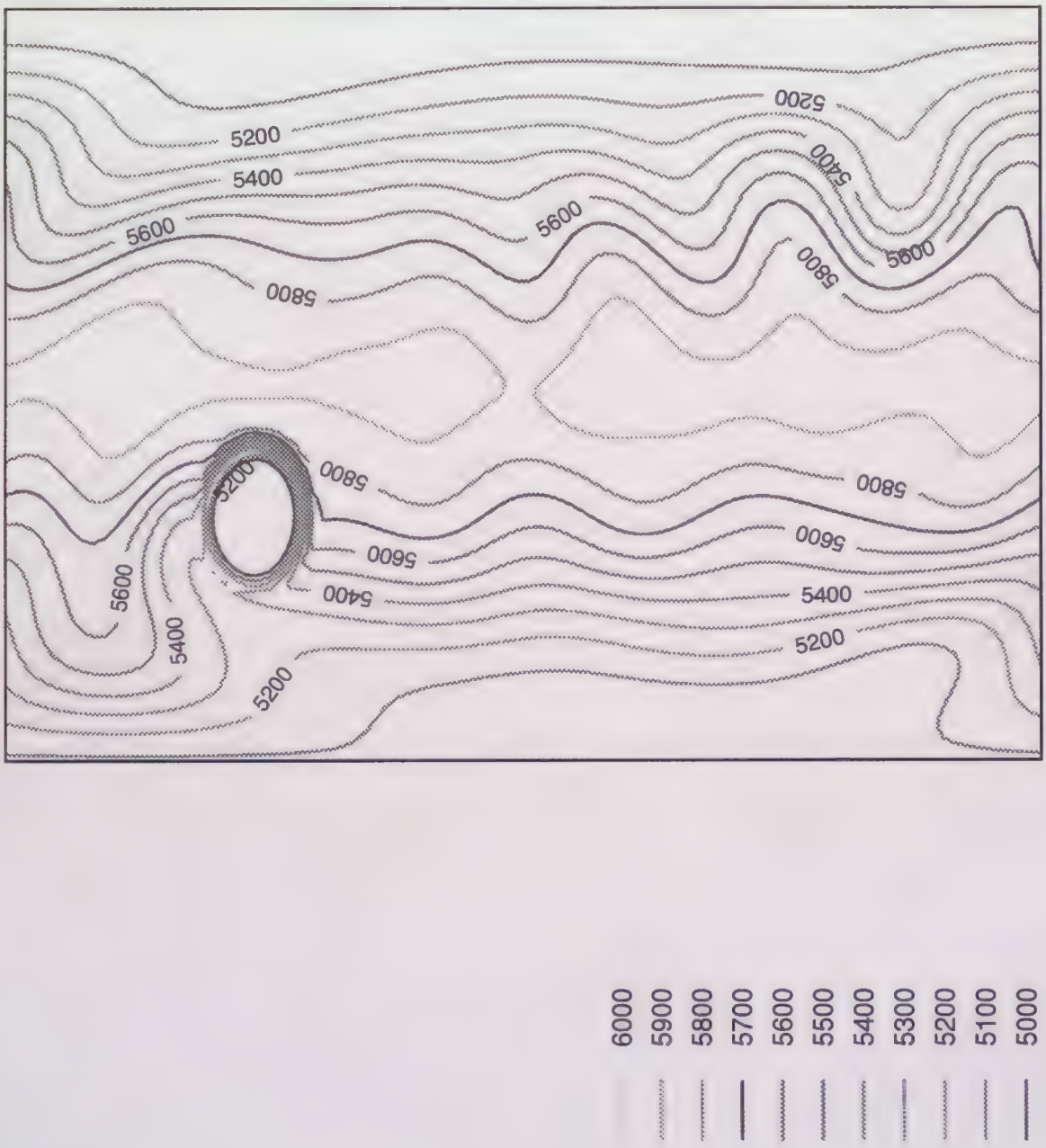

Figure 9: Test case 5, height field after 15 days

Figure 10: Test case 5, difference in height fields

Figure 11: Initial height field for test case 6

Figure 12: Reference solution after 14 days

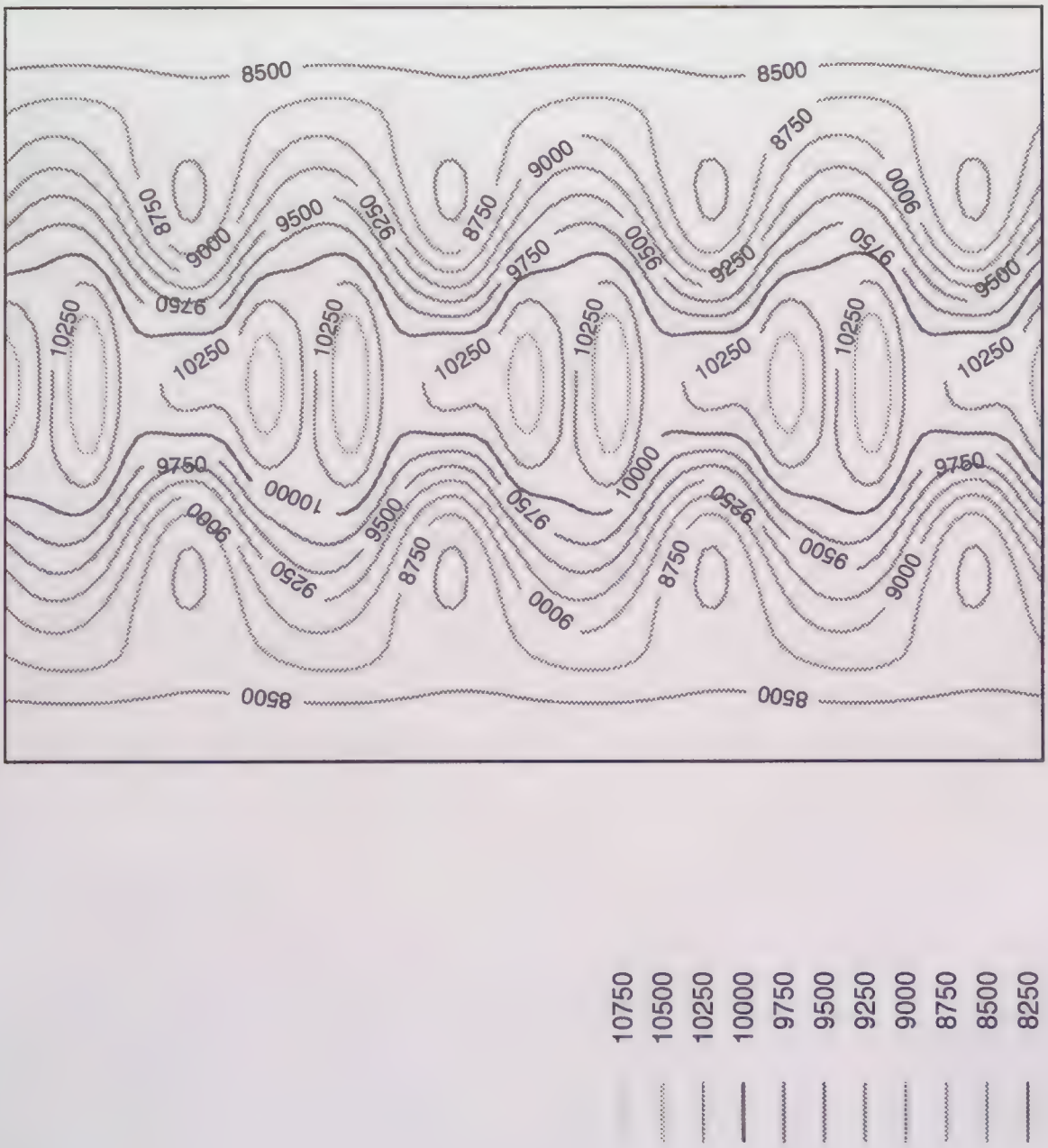

Figure 13: Solution after 14 days, filter fields, dt=10 minutes

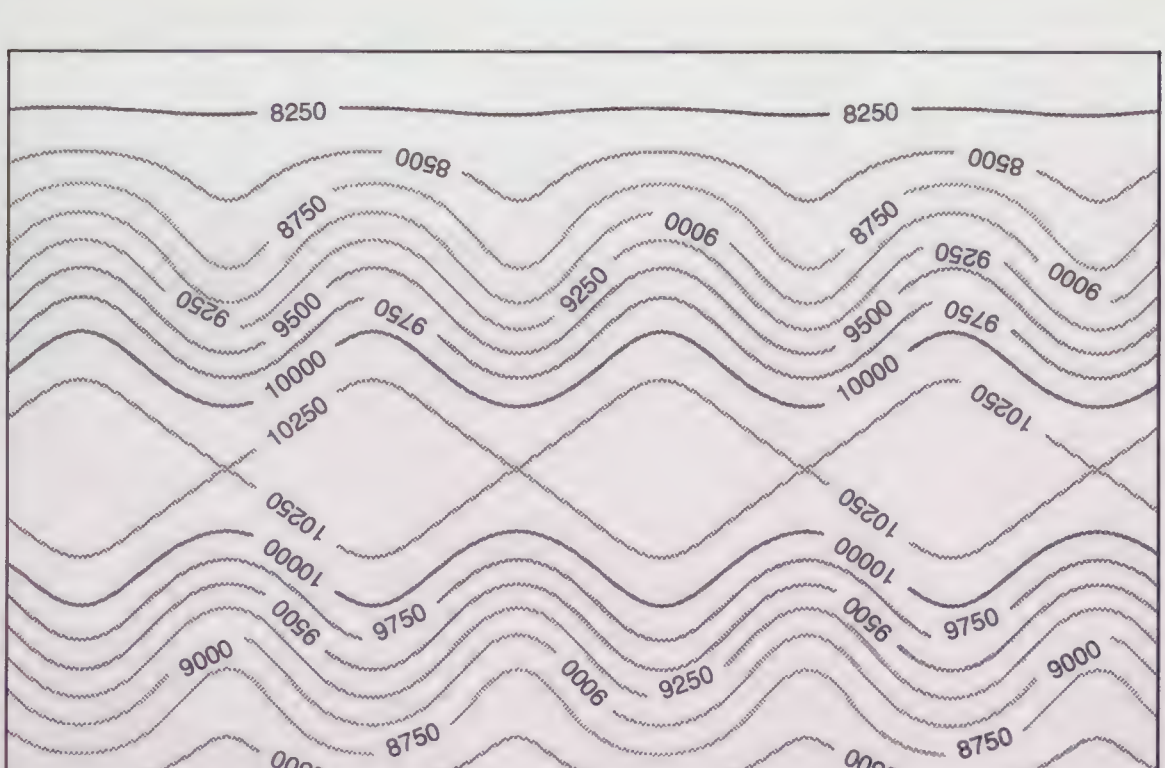

Figure 14: Solution after 14 days, filter fields, dt=1 minute

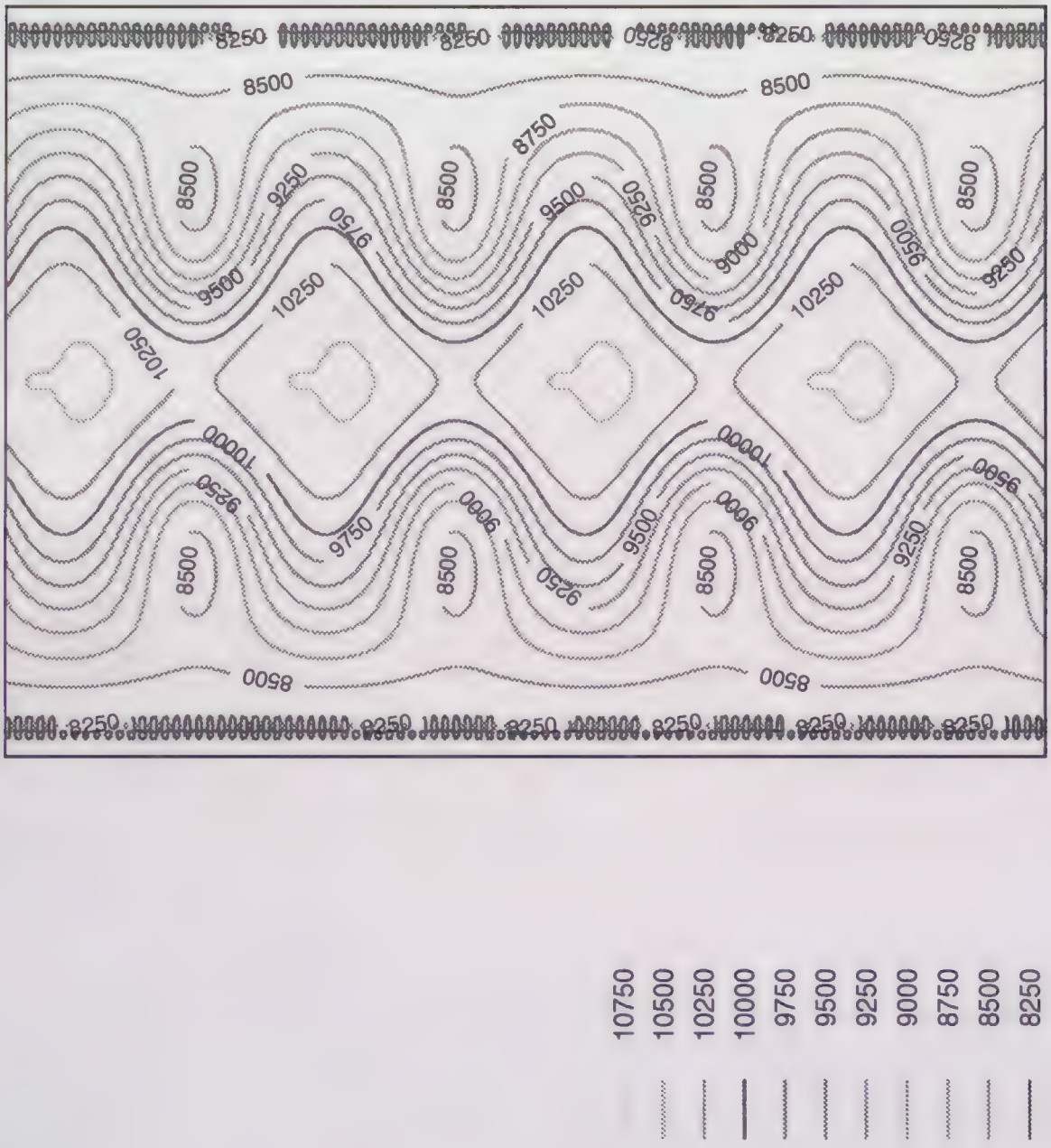

Figure 15: Solution after 14 days, filter fields, 288 x 217 grid, dt= 2 minutes

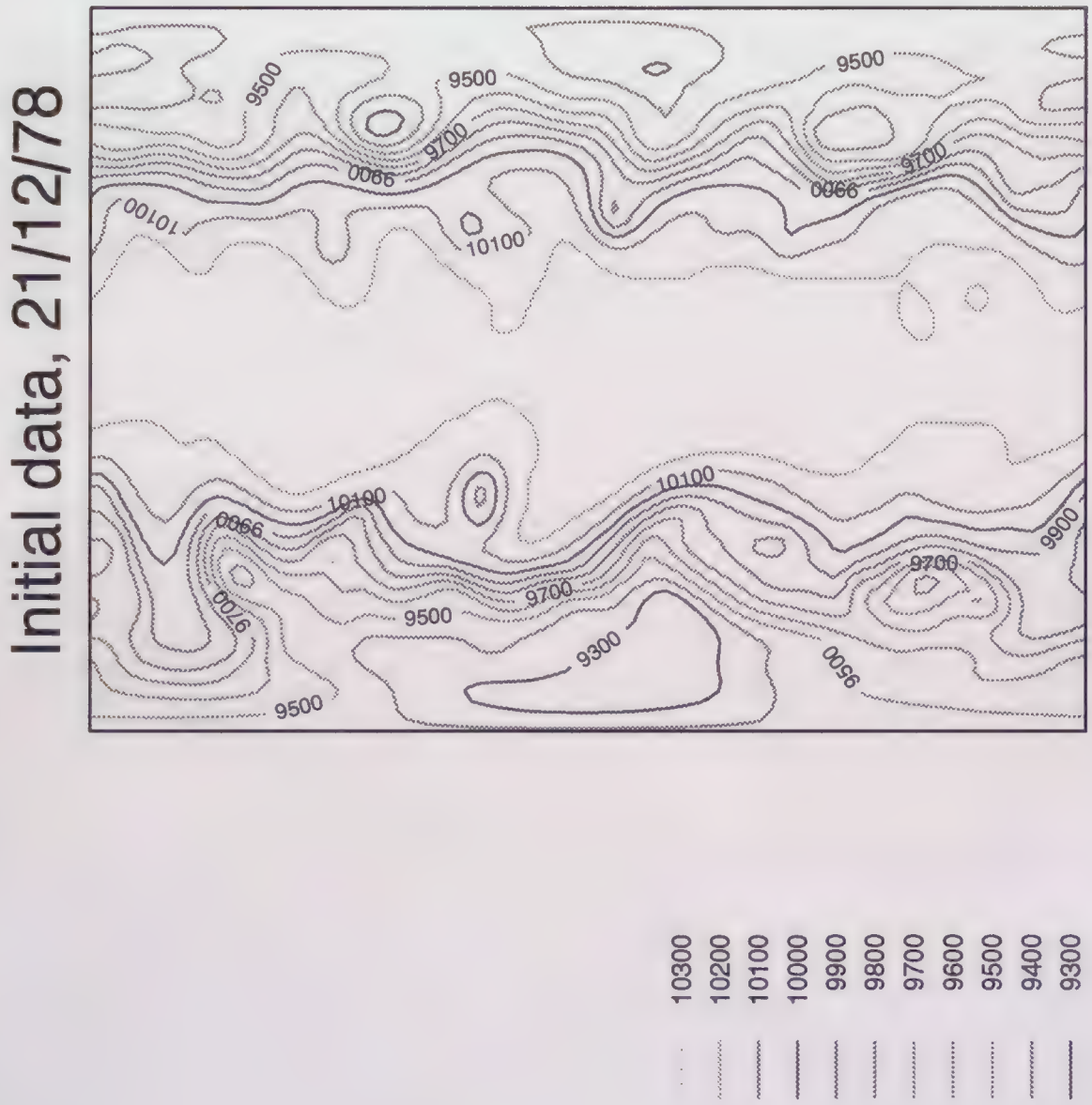

Figure 16: Initial height field for test case 7

Figure 17: Test case 7, reference solution height field after 5 days

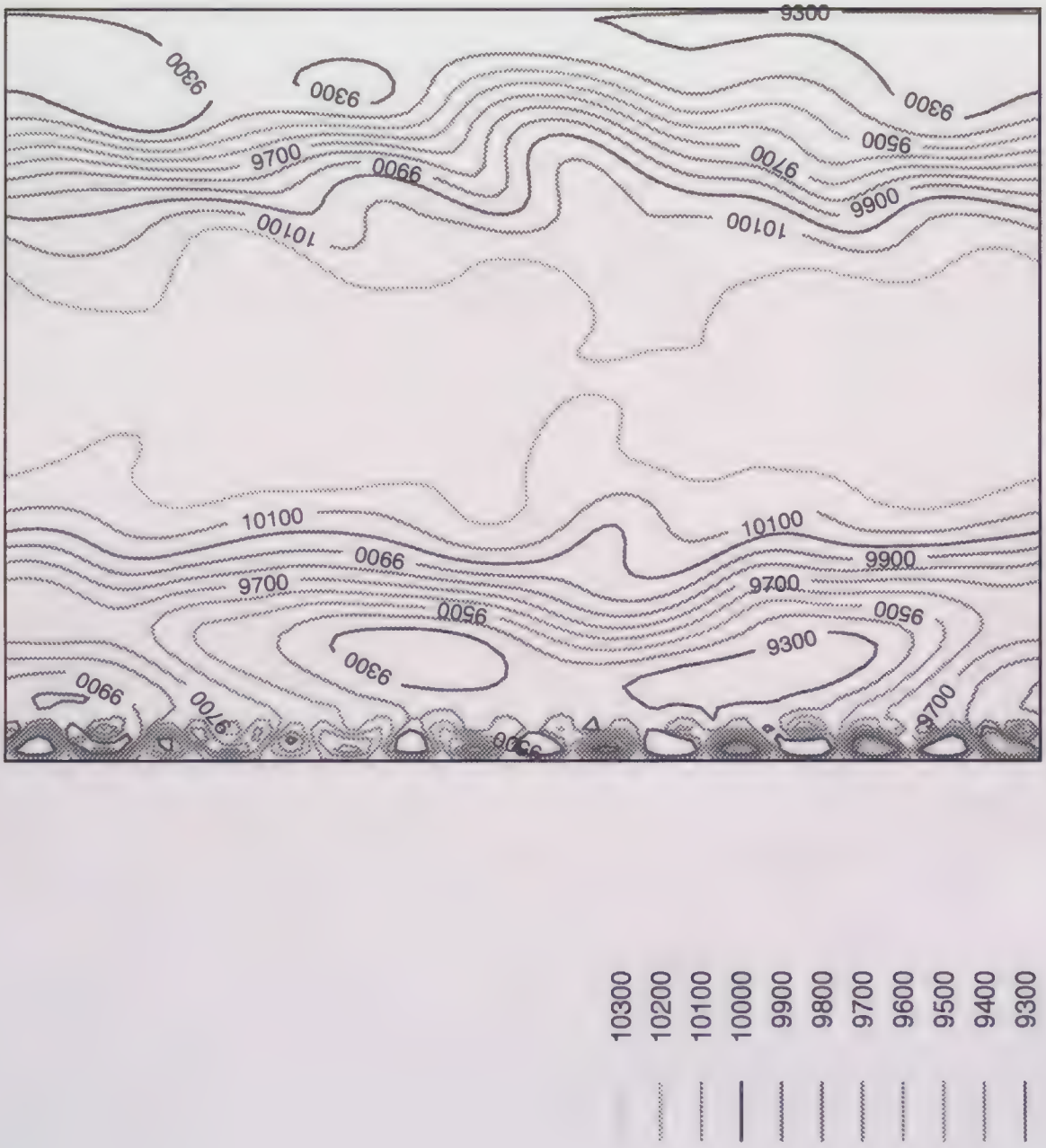

Figure 18: Test case 7, height field after 5 days

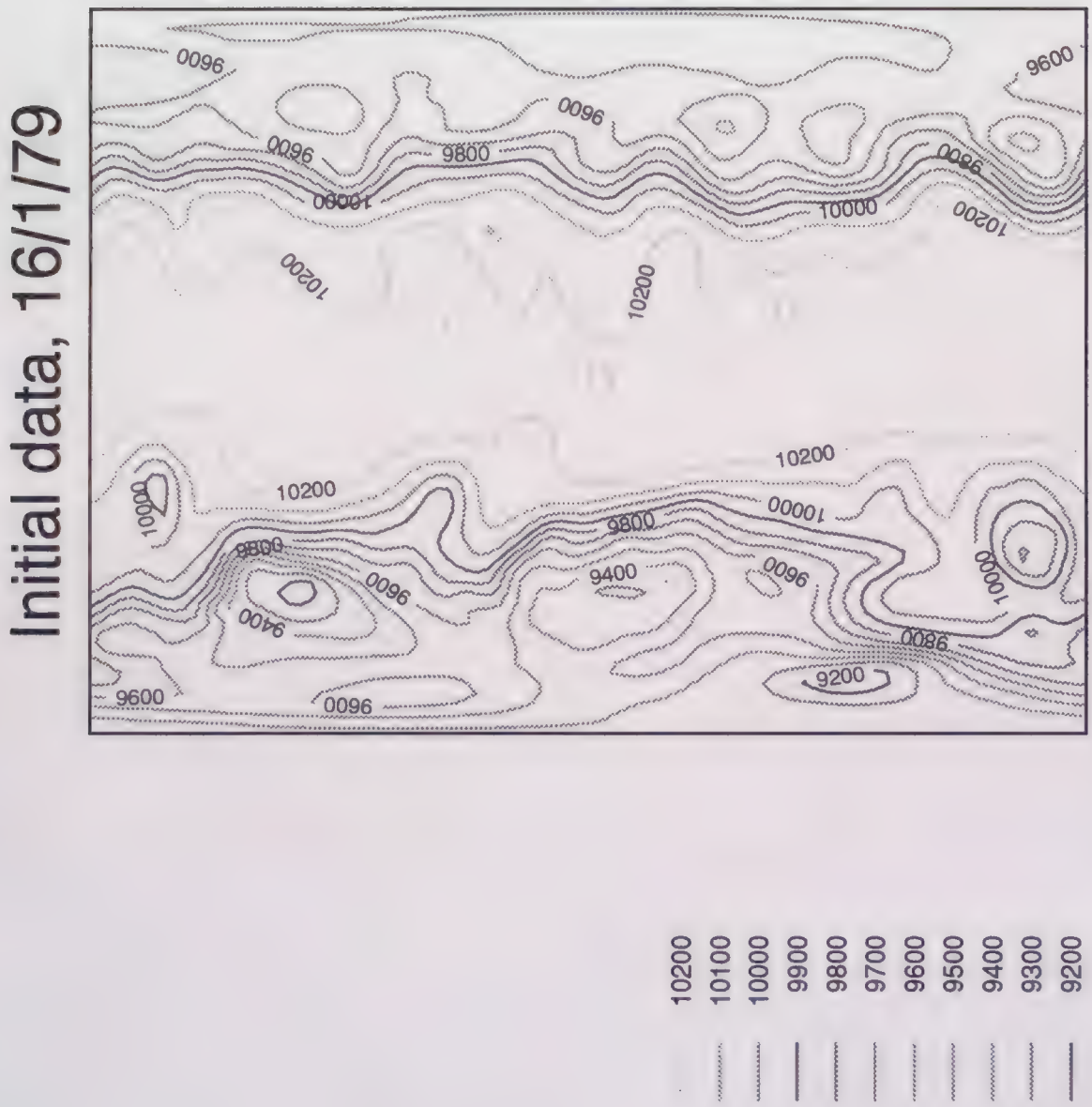

Figure 19: Initial height field for test case 7

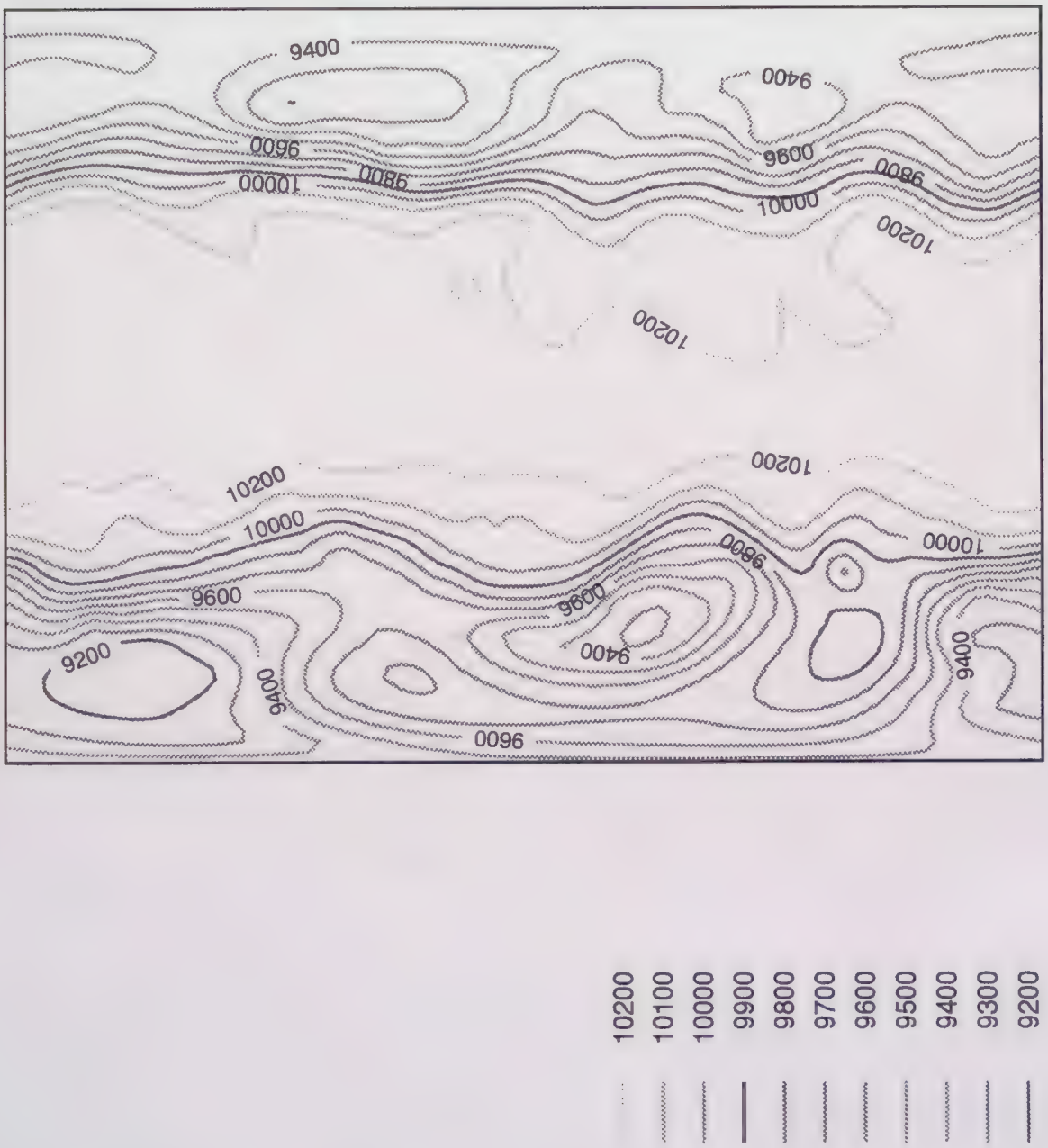

Figure 20: Test case 7, reference solution height field after 5 days

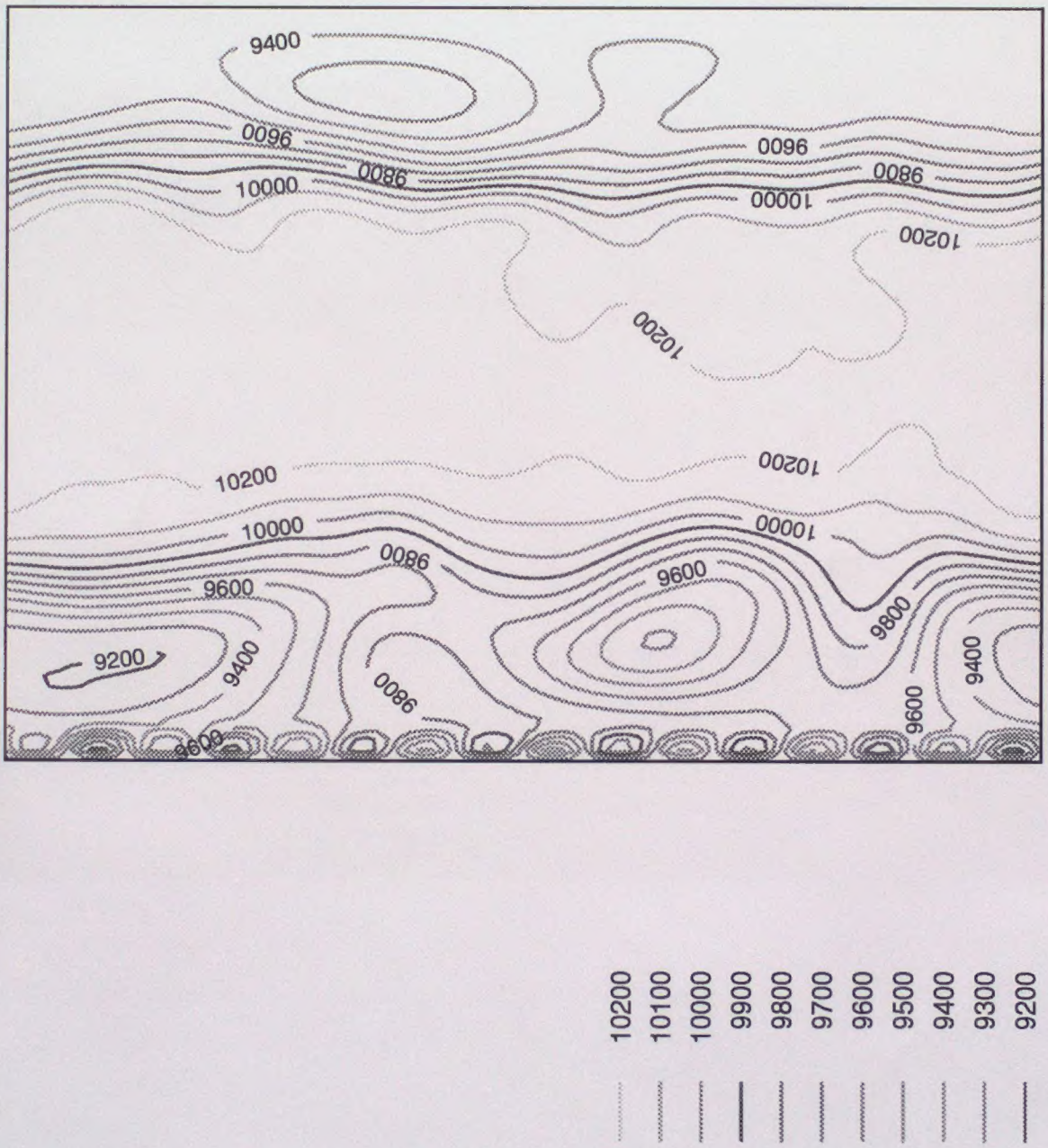

Figure 21: Test case 7, height field after 5 days

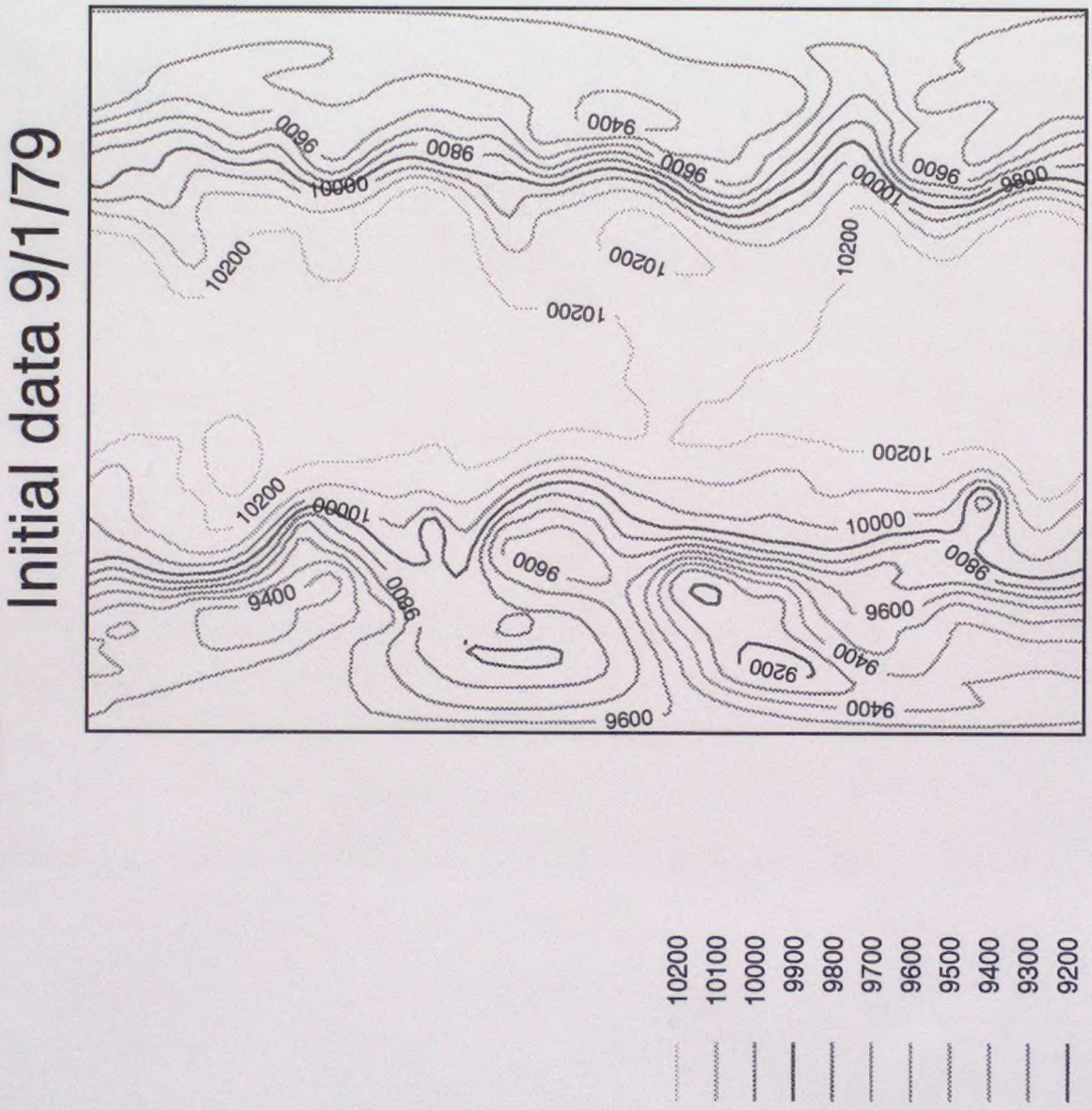

Figure 22: Initial height field for test case 7

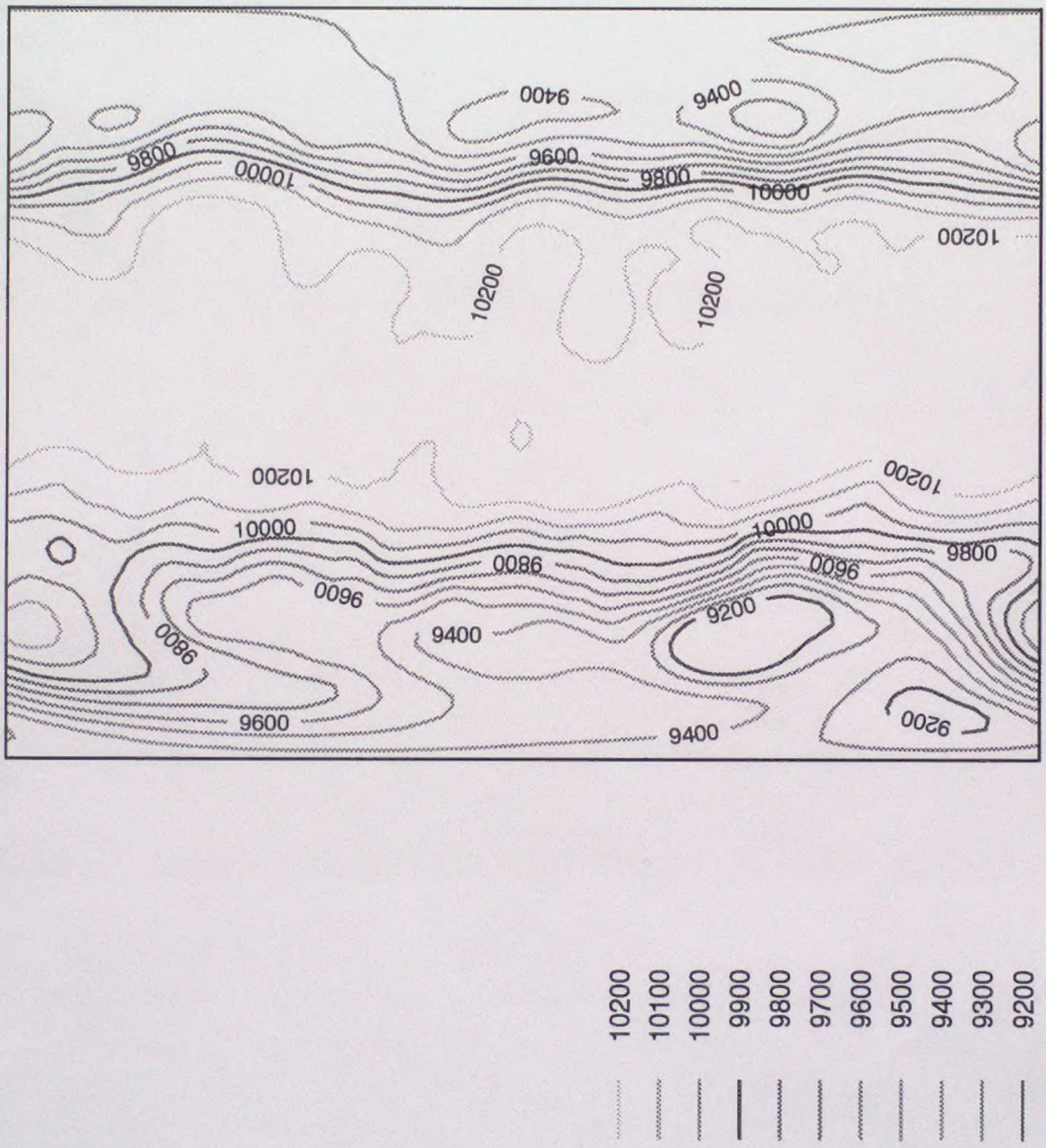

Figure 23: Test case 7, reference solution height field after 5 days

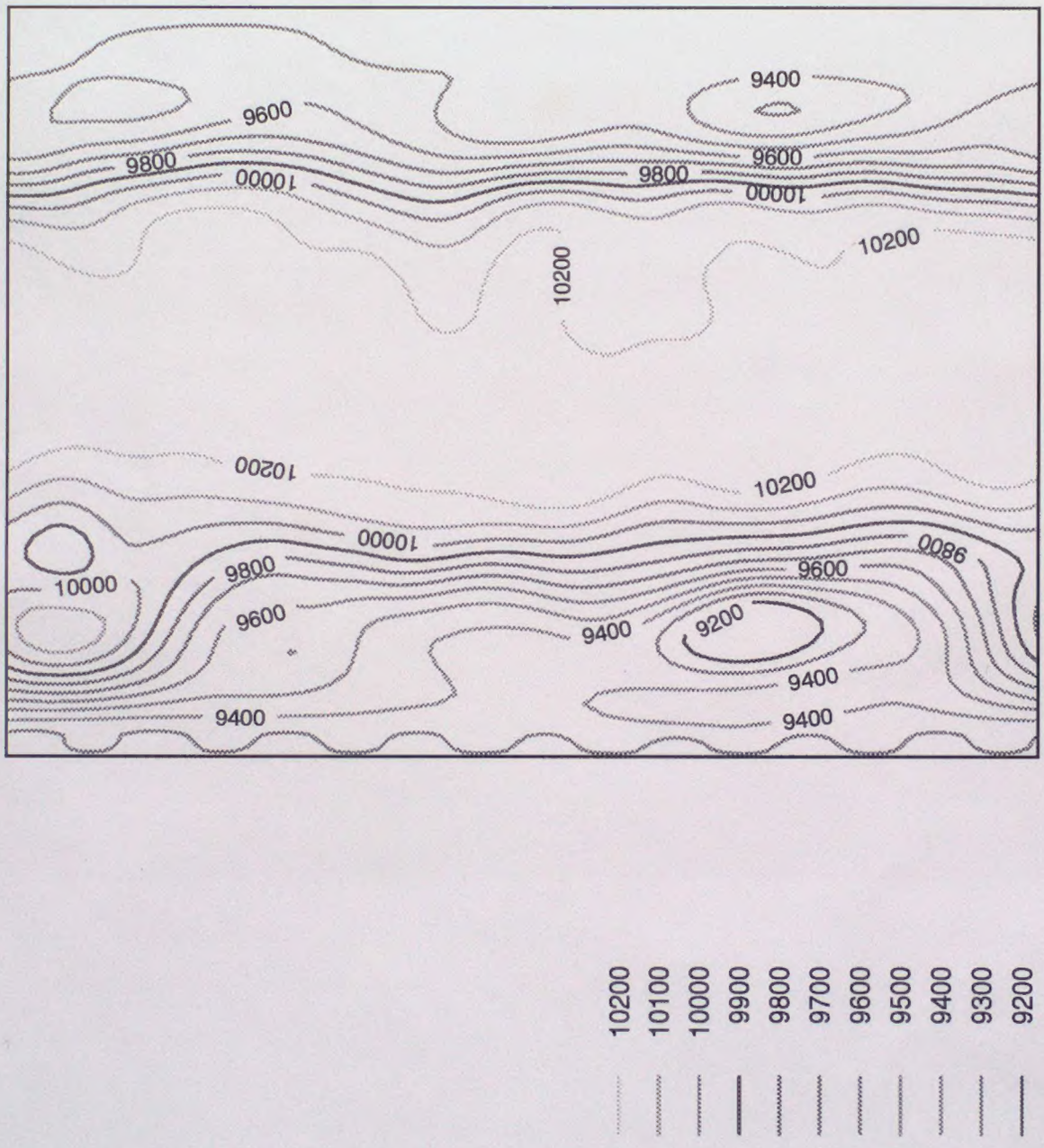

Figure 24: Test case 7, height field after 5 days